# Magnetization Measurements and Ginzburg-Landau Simulations of Micron-Size $\beta$-Tin Samples: Evidence for an Unusual Critical Behavior of Mesoscopic Type-I Superconductors

André Müller,[1] Milorad V. Milošević,[2] Sara E. C. Dale,[1] Miles A. Engbarth,[1] and Simon J. Bending[1]

[1]*Department of Physics, University of Bath, Claverton Down, Bath BA2 7AY, United Kingdom*
[2]*Departement Fysica, Universiteit Antwerpen, Groenenborgerlaan 171, B-2020 Antwerpen, Belgium*
(Received 18 May 2012; published 8 November 2012)

We describe investigations of the largely unexplored field of *mesoscopic type-I* superconductors. Micromagnetometry and 3D Ginzburg-Landau simulations of our single crystal $\beta$-tin samples in this regime reveal size- and temperature-dependent supercritical fields whose behavior is *radically different* from the bulk critical field $H_c^B$. We find that *complete suppression of the intermediate state* in medium-size samples can result in a surprising *reduction* of the critical field significantly below $H_c^B$. We also reveal an evolution of the superconducting-to-normal phase transition from the expected *irreversible* first order at low temperatures through the previously unobserved *reversible* first-order to a *second-order* transition close to $T_c$, where the critical field can be *many times larger* than $H_c^B$. Finally, we have identified striking correlations between the mesoscopic $H_{c3}$ for nucleation of surface superconductivity and the thermodynamic $H_c$ near $T_c$. All these observations are entirely unexpected in the conventional type-I picture.

The textbook description of a bulk type-I superconductor is one that exhibits perfect diamagnetism in fields up to the thermodynamic critical field $H_c^B$ when it undergoes a first-order transition to the normal state. In practice, real samples exhibit a very much richer range of phenomena, including intermediate states, surface superconductivity, supercooling, and superheating, and these were the subject of intense investigation in the 1950s, 1960s, and 1970s. Recent advances in sample fabrication, measurement, and imaging technology are allowing these problems to be revisited, and, in several cases, e.g., the competition between laminar and tubular intermediate state phases in *macroscopic* samples [1,2], our understanding is being radically revised. There has also been a resurgence of interest in *nanoscale* type-I samples whose radius $R$ is much smaller than the penetration depth $\lambda(T)$, in which huge enhancements of the critical field over the bulk value [$\approx (\lambda/R)H_c^B$] [3] have been reported. In stark contrast, the richest intermediate regime of *mesoscopic* type-I superconductivity, when sample dimensions are comparable to the superconducting coherence length $\xi(T)$, remains largely unexplored. In this Letter, we focus explicitly on this regime.

Mesoscopic superconductivity has been an extremely active area of research in recent years, but these studies have mostly focused on type-II superconductors or patterned disordered type-I superconducting films, which are often effectively in the type-II limit. Work on single crystal mesoscopic type-I samples has been largely restricted to resistance measurements of whiskers [4,5], where added voltage contacts are known to strongly perturb results [6] and distinguishing between Meissner and intermediate states is challenging. In order to bridge the *bulk* [$R \gg \xi(T)$] and *nanoscale* [$R \ll \lambda(T)$] regimes,

we have exploited recent breakthroughs in electrocrystallization on *B*-doped diamond electrodes [7], which allow the controllable growth of single crystal $\beta$-Sn rods with (sub)micrometer dimensions. Transfer to a Hall array micromagnetometer enables precise, contactless measurements of the magnetic response of *individual* Sn rods as a function of temperature and magnetic field. Figure 1(a) shows a scanning electron micrograph of a typical $\beta$-tin microcrystal on a *B*-doped diamond electrode. Approximately square cuboid-shaped rods were selected for investigation and sample dimensions accurately estimated from atomic force microscope images [cf., Fig. 1(b)]. Sample widths and lengths spanned the ranges $w \approx 0.7$–2.5 $\mu$m and $l \approx 0.9$–6.0 $\mu$m, respectively. The Ginzburg-Landau (GL) parameter of our $\beta$-tin samples is
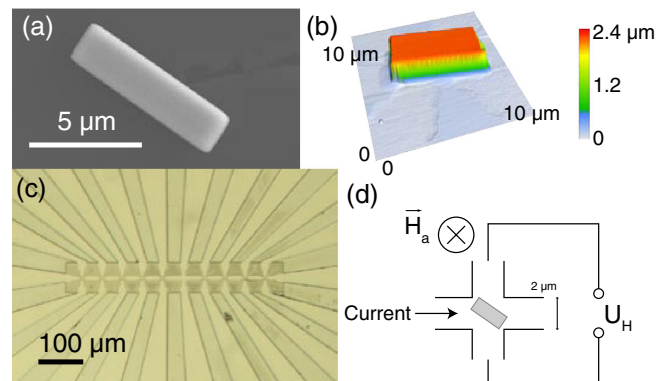


FIG. 1 (color online). (a) Scanning electron micrograph of a typical Sn rod deposited on a *B*-doped diamond electrode. (b) 3D atomic force microscope image of a Sn crystal mounted on a Hall probe. (c) Optical micrograph of a Hall probe array. (d) Sketch of the micromagnetometry measurement setup.

estimated to be [8] $\kappa(T_c) \cong 0.05\text{--}0.15 \ll 1/\sqrt{2}$, making this a model system for investigating the properties of strongly type-I superconductors. The critical temperature of all our rods is very close to the bulk value of $T_c = 3.72$ K, and the temperature-dependent thermodynamic critical field is well described by $H_c^B(T) = 306[1 - (T/T_c)^2]$ Oe. The low temperature magnetization of individual samples was measured by placing them directly on top of the 2 $\mu$m × 2 $\mu$m active elements of a GaAs/AlGaAs heterostructure Hall probe array [Fig. 1(c)] [9]. The Hall probes were driven with a 20 $\mu$A 314 Hz ac current and the Hall voltage detected by using two digital lock-in amplifiers [Fig. 1(d)] allowing the numerical subtraction of an active and an empty (reference) Hall element to obtain the *local* magnetization of the sample. Hall arrays were mounted on the end of a temperature-controlled sample holder that was coupled by exchange gas to a pumped liquid helium bath. An external magnetic field was applied perpendicular to the plane of the Hall array from a 1 T superconducting solenoid.

To verify the experimental findings, we employ 3D numerical GL calculations in a simulation region several times larger than the sample in all directions. To obtain the correct temperature dependence of $H_c^B \propto [1 - (T/T_c)^2]$, empirical modifications proposed by Ginzburg were used [10], so that the two GL equations read

$$(-i\vec{\nabla} - \vec{A})^2\Psi = \frac{1}{(1 - t^2)^2}(1 - t^4 - |\Psi|^2)\Psi \quad (1)$$

$$-\frac{\kappa(0)^2}{(1 + t^2)^2}\vec{\nabla} \times \vec{\nabla} \times \vec{A} = \text{Im}(\Psi^*\vec{\nabla}\Psi) - |\Psi|^2\vec{A}, \quad (2)$$

where all lengths are scaled to $\xi(0)$, the vector potential $A$ is expressed in units of $\Phi_0/2\pi\xi(0)$, the order parameter is scaled to its value at zero temperature and applied field, and $t = T/T_c$. As a consequence of these modifications, the GL parameter becomes temperature dependent; $\kappa(t) = \kappa(0)/(1 + t^2)$. The simulations are performed on a dense rectangular grid, with typically 5 grid points per $\lambda(T)$, with assumed parameters $\xi(0) = 174.5$ nm and $\kappa(0) = 0.25$, and the exact experimental $H_c^B(0) = 306$ Oe, $T_c = 3.72$ K, and sample dimensions. Neumann boundary conditions of the form $(-i\vec{\nabla} - \vec{A})\Psi|_n = 0$ are used at all surfaces [11].

Figure 2(a) shows magnetization data for three rods whose sizes span the full range investigated. The intermediate state was suppressed in all samples due to quantum confinement; the rods are considerably smaller than the equilibrium domain width $a = \sqrt{\delta d/f(\tilde{h})}$ for a laminar intermediate state structure, a periodic arrangement of straight superconducting, and normal domains. Here $\delta = (\xi - \lambda)$ is the wall energy parameter, $d$ is the sample thickness, and $f(\tilde{h}) = f_1(\tilde{h}) + f_2(\tilde{h}) < 0.023$ [12] is a function of reduced field and accounts for magnetostatic
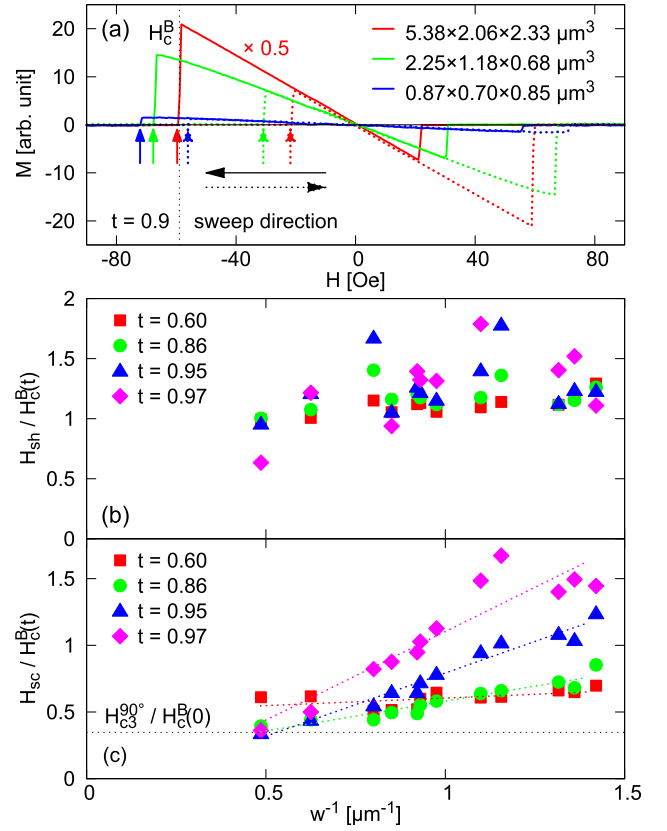


FIG. 2 (color online). (a) Local magnetization data at $t = T/T_c = 0.90$ for three different-sized Sn rods. The thermodynamic critical field $H_c^B(t = 0.90)$; $H_{sh}(t)$ (solid arrows) and $H_{sc}(t)$ (dashed arrows) are indicated. (b) The reduced superheating field $H_{sh}/H_c^B$ and (c) the reduced supercooling field $H_{sc}/H_c^B$, as a function of the inverse width $w^{-1}$ for different temperatures.

energy $[f_1(\tilde{h})]$ and the increased energy due to broadening of the normal domains at the sample surface $[f_2(\tilde{h})]$. For a typical sample thickness of $\approx 1$ $\mu$m we find $a > 2$ $\mu$m, and laminar domains are unstable for all investigated rod sizes. The data in Fig. 2(a) also show clear superheating of the superconducting state for sweeps to a higher field and supercooling of the normal state for sweeps to a lower field. The respective reduced supercritical fields are plotted against inverse rod diameter in Figs. 2(b) and 2(c) for many different samples at several reduced temperatures. Superheating in mesoscopic type-I samples has important applications; e.g., superheated superconducting granules are being developed as efficient high energy particle detectors [13,14]. $H_{sh}$ can be estimated theoretically as the highest field at which GL theory has a metastable solution under infinitesimal perturbations [15]. Analytic calculations of the superheating field in the limit of $\kappa \ll 1$ yield the approximate bulk result $H_{sh}^B \cong 2^{-1/4}\kappa^{-1/2}H_c^B$ [16]. Once $H_{sh}$ is reached at any point on the surface, a normal region begins to nucleate and the Meissner state is destroyed.

Consequently, a shape-dependent demagnetization factor $D$ has to be accounted for when discussing the results of Fig. 2(b), and the measured superheating field becomes $H_{sh} = (1 - D)H_{sh}^B$. With the field applied perpendicular to one of the long faces, $D$ depends only weakly on the rod length and has been estimated by using a formula due to Chen, Pards, and Sanches [17] for rectangular prisms. Substitution of the value $\kappa(0) = 0.25$ used in GL simulations into the $\kappa \ll 1$ limiting result given above yields $H_{sh}^B/H_c^B = 1.961$ for $t = 0.6$ (approximately in the bulk regime for all rods). Correcting this by the demagnetization factor ($D = 0.32$–$0.35$ [17]) in order to make a direct comparison with experiments, we obtain $H_{sh}^B/H_c^B = 1.27$–$1.33$, which is in reasonable agreement with the measured values in Fig. 2(b) for $t < 0.96$. In practice, the superheating fields plotted in Fig. 2(b) show lower and quite widely scattered values with no clear systematic dependence on rod width, and we conclude that nucleation of the normal state occurs at microscopic surface defects that are not detected by our characterization methods.

In contrast, we find that the supercooling fields (labeled $H_{sc}$) plotted in Fig. 2(c) are strongly enhanced in the narrowest rods and exhibit an approximately linear dependence on $1/w$ at high temperatures. It is well established that the normal state of type-I samples can be supercooled below $H_c^B$ to $H_{c2}$, at which point barriers to bulk nucleation vanish. Supercooling can, however, be restricted to the nucleation field for surface superconductivity if $H_{c3} < H_c^B$, as we show to be the case here. For a semi-infinite normal-superconducting planar interface, this nucleation field is calculated to be $H_{c3} \approx 1.695\sqrt{2}\kappa H_c^B$ [18]. It is known, however, that $H_{c3}$ strongly depends on the shape of the sample surface and is, in general, larger than this value. Schweigert and Peeters [19] have calculated $H_{c3}$ for wedge-shaped samples and, for 90° corners appropriate for our Sn rods, found $H_{c3}^{90°} \approx 1.97\sqrt{2}\kappa H_c^B$. Since this expression is independent of the sample width, it is clearly inconsistent with our results for supercooling fields in Fig. 2(c). In what follows, we argue that differences in $H_{sc}$ for crystals of different widths are a purely mesoscopic (i.e., size-dependent) effect as the width of the sample is decreased towards $\xi(T)$ and the confinement of the superconducting condensate starts to play a pronounced role. This is better illustrated in Fig. 3(a), which shows reduced critical field data as a function of temperature for a subset of three crystals (the smallest, the largest, and one of intermediate size). The coherence length of the condensate is increasing with temperature, and the influence of quantum confinement becomes more prominent at higher temperatures, as reflected in a rapid divergence of the reduced supercritical fields near $T_c$.

The results of our theoretical simulations are shown in Fig. 3(b) and correctly reproduce all the experimentally measured features. These include the ordering of the
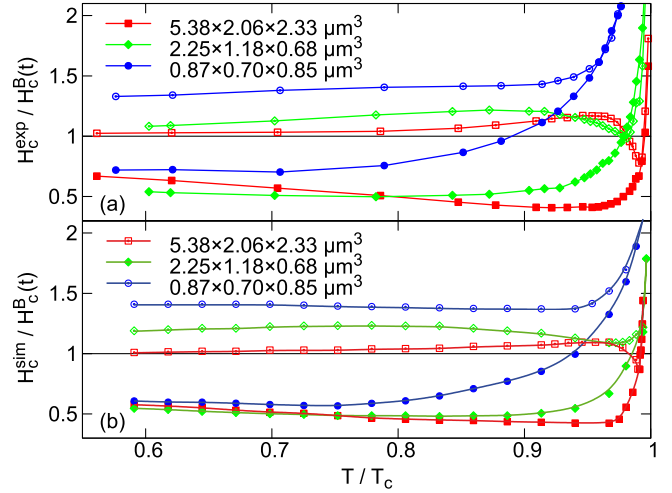


FIG. 3 (color online). (a) Comparison of the experimental supercooling (solid symbols) and superheating (open symbols) fields as a function of temperature and (b) the results of 3D GL calculations for a subset of three crystals.

curves for rods of different sizes, the crossover and convergence points, and the fall in $H_{sh}$ before its rise at high temperatures in the two larger crystals. Such behavior of $H_{sh}$ has been investigated numerically by Landau and Rinderer as a function of the width of superconducting slabs with a similar value of $\kappa$ [20]. $H_{sh}/H_c^B$ was initially found to fall as the width decreased below $20\lambda(T)$, then pass through a minimum at $w_c \approx 4\lambda(t)$, and rise again for still narrower slabs. Using $\lambda(t) = 43.65 \text{ nm}/\sqrt{1 - t^4}$ from our GL model, we estimate that our intermediate rod will reach $w = w_c$ for $t = 0.994$, which is significantly higher than in our data ($t = 0.979$) and the GL simulation ($t = 0.973$) due to the finite (and strong) longitudinal confinement in our samples at high temperatures. Remarkably, we also see that the superheating field of the largest rod actually falls *below* the bulk critical field for a narrow range of temperatures around $t = 0.98$ in both experimental and theoretical plots. This has its origin in the suppression of the intermediate state in these mesoscopic rods, which prevents the system from reducing enhanced surface fields due to finite demagnetization factors. As a consequence, superconductivity is actually quenched at lower fields in these mesoscopic samples than it would be in bulk samples. While we believe that our isotropic GL model captures the essential physics of the problem, the properties of Sn are known to be quite strongly anisotropic, and any discrepancies between theory and experiment can probably be attributed to this. To obtain further insights into the physics at play, we analyze our results in terms of available *analytic* theories. The shallow downward trend of $H_{sc}/H_c^B$ at lower temperatures in Fig. 3 falls outside the mesoscopic regime when our crystals are significantly larger than the superconducting length scales and agrees well with the prediction for wedges with 90° corners given

above, $\tilde{h} = H_{c3}^{90°}/H_c^B$ [19], after inclusion of the temperature dependence of the GL parameter [cf., lower solid line in Fig. 4]. In general, the nucleation of the superconducting state in large cuboid rods $w \gg \xi(T)$ occurs at the value of $H_{c3}$ for which the maximum of the superconducting order parameter lies approximately $\xi(T)$ inside the sample surface. Ginzburg and Landau have analyzed the related problem of a thin slab [21] and found that, above the temperature at which the critical width $w_0 = 1.84\xi(T)$ is reached, the two opposing surfaces couple and superconductivity nucleates in the center of the slab rather than just below the surface. Assuming that $\xi(0) = 230$ nm in the direction of interest [22], a predicted rise in $H_{sc}/H_c^B$ of our smallest rod for $T > 0.75T_c$ is in excellent agreement with the behavior observed in Figs. 3(a) and 3(b). For $w \ll \xi(t)$ Ginzburg and Landau showed that the second-order transition just below $T_c$ was described by $H_c(t)/H_c^B(t) \approx \sqrt{24}\lambda(t)/w$, and subsequent numerical work by Fink [23] revealed that the same expression accurately describes $H_{c3}(t)$ in the very much broader temperature region $w < 1.6\xi(t)$. Hence, remarkably, we anticipate that the supercooling field at low temperatures and the second-order transition field near $T_c$ should be described by a single common curve in our samples. Silin [24] has used GL theory to investigate the critical fields of mesoscopic type-I superconducting cylinders and spheres and demonstrated that the superconducting-normal transition becomes second order when $r_0 = R/\lambda(t) < \sqrt{3}$ (cylinders) and $r_0 < \sqrt{21}/2$ (spheres), where $R$ is the radius of the sample. In this limit $H_c/H_c^B \approx \sqrt{8}/r_0$ and $H_c/H_c^B \approx 2\sqrt{5}/r_0$ for cylinders and spheres, respectively. The reduced supercooling fields plotted in Fig. 2(a) appear to exhibit this inverse width ($w = 2R$) relationship at high temperatures. If we analyze the $t = 0.97$ data in this way, we extract a penetration depth that is about a factor of 2 too large for the cylinder model [$\lambda(0)_{\text{eff}} = 78 \pm 10$ nm] and is

almost exactly correct for the sphere model [$\lambda(0)_{\text{eff}} = 49 \pm 5$ nm], even though most of the data points are not strictly in the limit of Silin's theory. We argue that the sphere model is actually more appropriate for our samples, since (i) the smallest rods investigated are almost cubic in shape and (ii) our samples exhibit strong quantum confinement along the length of the rods. Figure 4 shows the raw supercritical fields in the high temperature part of the phase diagram for the smallest and largest rods, revealing that $H_{sc}$ for the biggest rod is well described by $H_{c3}^{90°}(t)$ for $t < 0.95$. We see that $H_{sh}$ and $H_{sc}$ significantly exceed $H_c^B$ close to $T_c$ and eventually converge on each other at the temperature where the transition becomes reversible. Careful examination of the $M(H)$ loops for the smallest rod shown in Fig. 5 indicates that the system initially enters a first-order reversible regime with a finite magnetization jump at $H_c$ for $t > 0.964$ before becoming continuous second-order for $t > 0.974$, rather close to the predicted onset of the second-order regime calculated by Silin ($t = 0.979$ for our system). The onset of a continuous transition signals the start of the extremely confined *nanoscale* regime, where screening of the magnetic field is incomplete and the concept of type-I superconductivity no longer applies. As anticipated above, we find that the $r_0 < \sqrt{21}/2$ limit theory for spherical mesostructures almost perfectly describes the supercooling branch of the data for the smallest rod from $t < 0.8$ where the transition is highly irreversible all the way up to $T_c$, where the transition is continuous and reversible (cf., Fig. 4). This, and the linear behavior of Fig. 2(c) at high temperatures, conclusively demonstrates for the first time the link between the supercooling field and $H_{c3}(t)$ at low temperatures and $H_c(t)$ in the reversible regime near $T_c$.

In conclusion, we present systematic measurements of supercritical fields in *individual* 3D mesoscopic type-I superconductors. We show that their supercooling and superheating fields can greatly exceed the bulk critical field $H_c^B$ in sufficiently small samples or at sufficiently high temperatures when the sample size becomes comparable to the temperature-dependent coherence length and strong quantum confinement sets in. Paradoxically, the superheating field for intermediate-sized rods is unexpectedly found
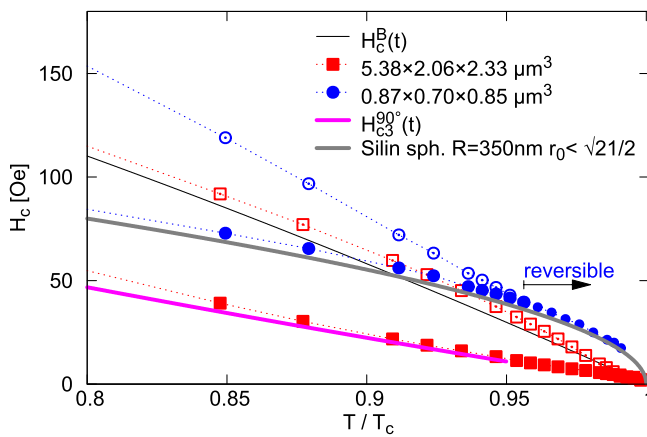


FIG. 4 (color online). Superheating (open symbols) and supercooling (solid symbols) fields near $T_c$ for the smallest and largest Sn crystals, in comparison with analytic formulas.
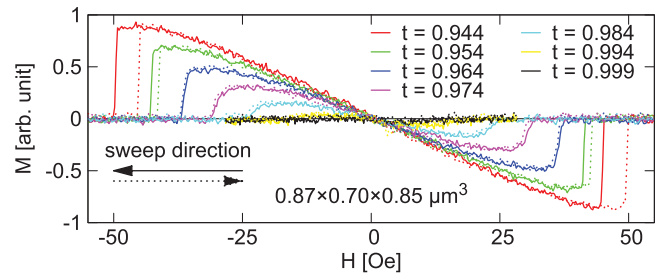


FIG. 5 (color). $M(H)$ loops near $T_c$ for the smallest crystal in Fig. 4 illustrating the change from an irreversible to a reversible transition as the temperature is increased.

to fall substantially below $H_c^B$ over a narrow temperature window due to quantum suppression of the intermediate state. Magnetization loops for individual rods reveal a surprisingly broad region where the transition is reversible; the classical irreversible (type-I) first-order signal-to-noise transition at low temperatures initially evolves into a hitherto unobserved reversible first-order, and then continuous second-order, transition as the temperature increases. We conclusively demonstrate that the low temperature supercooling field is set by $H_{c3}(t)$ for nucleation of surface superconductivity and remarkably reveal that $H_{sc}(t)$ at low temperatures and $H_c(t)$ in the reversible second-order region near $T_c$ are described by a single common curve. These are just the initial findings in the field of small type-I superconductors, which promises to reveal physics as rich as its type-II counterpart.

[1]  R. Prozorov, A. F. Fidler, J. R. Hoberg, and P. C. Canfield, Nat. Phys. **4,** 327 (2008).

[2]  R. Prozorov, Phys. Rev. Lett. **98,** 257001 (2007).

[3]  J. E. Han and V. H. Crespi, Phys. Rev. B **69,** 214526 (2004).

[4]  O. Lutes, Phys. Rev. **105,** 1451 (1957).

[5]  W. Webb and R. Warburton, Phys. Rev. Lett. **20,** 461 (1968).

[6]  D. Lucot, F. Pierre, D. Mailly, K. Yu-Zhang, S. Michotte, F. de Horne, and L. Piraux, Appl. Phys. Lett. **91,** 042 502 (2007).

[7]  A. Müller, S. E. C. Dale, M. A. Engbarth, S. J. Bending, and L. M. Peter, CrystEngComm **12,** 2135 (2010).

[8]  K. Zemmour and K. Saidi, Thin Solid Films **424,** 253 (2003).

[9]  A. K. Geim, S. V. Dubonos, J. G. S. Lok, I. V. Grigorieva, J. C. Maan, L. T. Hansen, and P. E. Lindelof, Appl. Phys. Lett. **71,** 2379 (1997).

[10]  V. L. Ginzburg, Sov. Phys. JETP **3,** 621 (1956).

[11]  M. Milošević and R. Geurts, Physica (Amsterdam) **470C,** 791 (2010).

[12]  L. Landau and E. Lifshitz, *Electrodynamics of Continuous Media* (Pergamon, New York, 1960).

[13]  A. Larrea, A. Morales, G. Waysand, and J. Bartolomé, Nucl. Instrum. Methods Phys. Res., Sect. A **317,** 541 (1992).

[14]  A. Larrea, J. Bartolomé, A. Morales, J. Morales, and G. Waysand, J. Magn. Magn. Mater. **104–107,** 229 (1992).

[15]  H. J. Fink and A. G. Presson, Phys. Rev. **182,** 498 (1969).

[16]  Orsay Group on Superconductivity, *Quantum Fluids, Proceedings of the Sussex University Symposium 1965* (North-Holland, Amsterdam, 1966).

[17]  D.-X. Chen, E. Pards, and A. Sanches, IEEE Trans. Magn. **38,** 1742 (2002).

[18]  D. Saint-James and P. G. Gennes, Phys. Lett. **7,** 306 (1963).

[19]  V. A. Schweigert and F. M. Peeters, Phys. Rev. B **60,** 3084 (1999).

[20]  I. L. Landau and L. Rinderer, J. Low Temp. Phys. **100,** 219 (1995).

[21]  V. L. Ginzburg and L. D. Landau, Zh. Eksp. Teor. Fiz. **20,** 1064 (1950).

[22]  P. C. L. Tai, M. R. Beasley, and M. Tinkham, Phys. Rev. B **11,** 411 (1975).

[23]  H. J. Fink, Phys. Rev. **177,** 1017 (1969).

[24]  V. P. Silin, J. Exp. Theor. Phys. **21,** 1330 (1951).